

Interdigitating Organic Bilayers Direct the Short Interlayer Spacing in Hybrid Organic–Inorganic Layered Vanadium Oxide Nanostructures

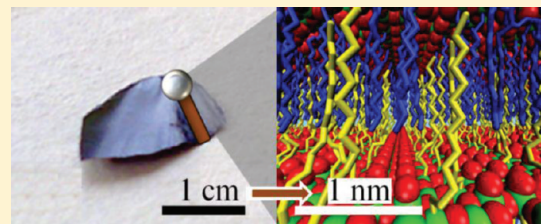
G. Gannon,^{†,§} C. O'Dwyer,^{*,‡} J. A. Larsson,[†] and D. Thompson^{*,†}

[†]Theory Modelling and Design Centre, Tyndall National Institute, University College Cork, Cork, Ireland

[‡]Department of Physics and Energy, Materials and Surface Science Institute, University of Limerick, Limerick, Ireland

 Supporting Information

ABSTRACT: Layered metal oxides provide a single-step route to sheathed superlattices of atomic layers of a variety of inorganic materials, where the interlayer spacing and overall layered structure forms the most critical feature in the nanomaterials' growth and application in electronics, health, and energy storage. We use a combination of computer simulations and experiments to describe the atomic-scale structure, dynamics and energetics of alkanethiol-intercalated layered vanadium oxide-based nanostructures. Molecular dynamics (MD) simulations identify the unusual substrate-constrained packing of the alkanethiol surfactant chains along each V₂O₅ (010) face that combines with extensive interdigitation between chains on opposing faces to maximize three-dimensional packing in the interlayer regions. The findings are supported by high resolution electron microscopy analyses of synthesized alkanethiol-intercalated vanadium oxide nanostructures, and the preference for this new interdigitated model is clarified using a large set of MD simulations. This dependency stresses the importance of organic–inorganic interactions in layered material systems, the control of which is central to technological applications of flexible hybrid nanomaterials.



INTRODUCTION

Many emerging applications of nanostructures involve organic molecules adsorbed on inorganic substrates.¹ Organic functionalization, monolayer formation and docking onto inorganic substrates has been a key building block interaction that has allowed control over size, shape, physicochemical properties, and assembly. As an important subset to the rational design of many nanostructures through organic–inorganic interactions and assemblies, the role of the surfactant packing and adsorption onto the inorganic phase is crucial in order to influence crystal growth and assembly.^{2,3} The vast majority of such interactions concern the synthetic control of nanocrystals and nanowires, but incorporation of these structure-influencing organic layers into the crystals such as layered double hydroxides⁴ and layered metal oxide materials is mostly limited to variations in the type of organic intercalant, and much less is known about the influence of this phase and its interaction on the overall layered material. The advantage of template-based growth methods is the ability of fabricating unidirectionally aligned and uniformly sized nanostructured arrays. To this end, the direct engineering of complex nanostructures is highly desirable, but controlled hierarchical structuring of choice materials remains challenging.^{5,6}

Layered metal oxides with characteristic morphologies similar to single crystal nanostructures, such as nanofibers, provide a single-step route to sheathed superlattices of atomic layers of inorganic material⁷ and have applications ranging from energy-storage, display devices, (photo)electrochromic devices, electrocatalysis, and photovoltaics to novel energy-conversion systems, proton-pump electrodes, and sensors, for example, chemiresistive

artificial nose detectors.^{8–13} The motivation for the present study stems from the considerable attention that these layered nanostructures are currently receiving,¹⁴ coupled to the limited knowledge on the true effect of intercalated organic monolayers on structure and physicochemical properties.^{15–17} Vanadium oxide is re-emerging with renewed interest, based on its layered architecture and the possibility of its application to energy storage and conversion¹⁸ among many other beneficial properties.¹⁹ For example, the influence of the soft organic phase was shown to influence specific charge capacity and cycle life in vanadate-based lithium-ion battery materials.¹³ As a layered transition metal oxide, it also serves as a model material for hybrid organic–inorganic nanomaterial investigations.

In the present work, we resolve the structure of alkanethiol-vanadium oxide hybrid materials, both experimentally and theoretically. We use a combination of electron microscopy imaging and atomic-resolution molecular dynamics simulations to clarify the role of surfactant molecules in the assembly of layered metal oxide nanostructures, which go beyond known experimental and computational tandem approaches that primarily focused on phase changes in the harder inorganic phase.²⁰ We show that alkanethiol molecules self-assemble preferentially in a vertically interdigitated, bilayered arrangement between the layers comprising the vanadium oxide-based nanostructures.²¹ The findings demonstrate that a controlled interlayer spacing in a layered

Received: August 11, 2011

Revised: October 25, 2011

Published: October 31, 2011

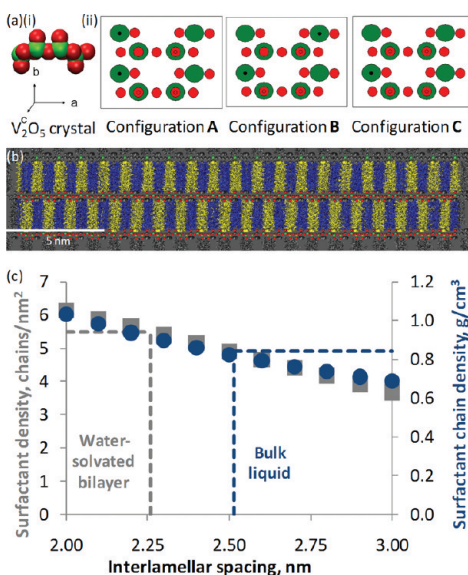


Figure 1. Panel a (i) shows the V_2O_5 unit cell,³⁰ composed of a V_4O_{10} repeat unit with lattice parameters $a = 11.51$, $b = 3.56$, and $c = 4.37 \text{ \AA}$ (space group $Pmmn$), together with (ii) plan view schematics of V_2O_5 (010) functionalized with three alternative alkanethiol attachment configurations: A, B, and C. Black full circles represent alkane chains pointing up, and black empty circles represent alkane chains pointing down. Panel b shows one representative computed nanofiber structure, for configuration A with interlamellar space of 2.0 nm. Chains on the opposite substrate faces are colored blue and yellow. Surrounding periodic images are colored gray. Panel c shows how chain density changes with interlamellar spacing. The square and circular data points (lefthand and righthand axes) show the change in chain packing densities, expressed as chains/ nm^2 and g/cm^3 ; the gray and blue dashed lines mark the computed chain density in the reference water-solvated bilayer and bulk liquid.

material can be obtained by the incorporation of the organic bilayer. The interlayer spacing is dependent not only on the length of the alkyl chain and how they interact but also on the density of organic molecules on the surface of the inorganic phase and how the overall packing density maintains interlayer spacing throughout the layer, even when grown as a superlattice of many organic–inorganic bilayers stacked periodically back-to-back.

MATERIALS AND METHODS

Characterization of Vanadium Oxide-Alkanethiol Nanofibers. Details on the synthesis of the vanadium oxide-thiol nanofibers are outlined in detail elsewhere.^{21,22} X-ray powder diffraction characterization was performed using a SIEMENS D5000 diffractometer ($\text{Cu K}\alpha = 0.15418 \text{ nm}$; operation voltage, 40 kV; current, 30 mA). Transmission electron microscopy (TEM) was conducted using a JEOL 2100F FEGTEM operating at 200 kV. X-ray photoelectron spectroscopy was performed using a Kratos Axis 165 equipped with a monochromatic Al source ($\text{K}\alpha 1486.58 \text{ eV}$) with a spot size of 1 mm. The source power was 150 W, the takeoff angle was set normal to the sample surface, the construction and peak fittings in the narrow region spectra were performed using a Shirley type background, and the synthetic peaks were of a mixed Gaussian–Lorentzian type. Adventitious carbon was used for the charge reference, and the C 1s line of adventitious hydrocarbon was assumed to have a binding energy of 284.8 eV. After synthesis, dried xerogel

samples comprising nanofibers were stored under 1 atm with a relative humidity of 40%. No humidity control was used during analytical (diffraction/microscopic) measurements due to vacuum requirements.

Choice of Thiol-Substrate Binding Sites. Three alternative grafting arrangements were considered in the molecular models (Figure 1), differing in the (experimentally unknown) local distribution of the thiol attachment sites. The molecule surface attachment sites on the V_2O_5 substrate in the model involve the thiol headgroups binding via the negatively charged S atom to the vanadium Lewis acid sites at the V_2O_5 (010) surface,²³ so we bound alkanethiols to sterically accessible vanadium sites, those without a doubly bound oxygen sitting on top. There are many other possibilities, involving alternative surface binding sites as a consequence of, for example, thiol molecules adsorbing via -SH instead of -S headgroups to doubly bonded vanadyl oxygens and/or surface in-plane nucleophilic oxygens,²⁴ oxygen vacancies, surface V^{5+}/V^{4+} ratios, and new surface states formed following, for example, condensation reactions.²⁵

The representative model we chose may also serve as a first approximation to the alternative alkylamine- V_2O_5 lamellar structure,²¹ the doubly bonded vanadyl oxygens serving as likely candidates for NH_3^+ binding sites. In Figure S1 of the Supporting Information, we show a HRTEM image of the layered walls of a dodecylamine-templated V_2O_5 nanotube,^{13,26} which routinely show an interlayer spacing of 2.65–2.7 nm. The increase in interlamellar separation from 2.5 (thiol templated) to ~2.7 nm (amine templated) corresponds to an increase of 1–2 V=O bond lengths. Hence, a similar film horizontal lattice constant may be expected for alkyl amines as for alkanethiols. Note, however, the further discussion of the lamellar structural features are associated with more mobile ionic, e.g., NH_3^+ , anchor groups in ref 27. In common with alkanethiol adsorption described above, alternative film–substrate binding sites are also possible for alkylamines, in particular due to competition^{24,28} between the surface Bronsted base V=O and in-plane Lewis base V–O–V oxygens for the amino headgroups.

An important additional model feature is that we restricted ourselves in this study to structures with all alkanethiols chemically bound to the substrate, given the strong energetic benefit of a thiol/substrate chemisorption of at least 20 kcal/mol,²⁹ which is generally much larger than the magnitude of the film packing effects calculated in this study (Table 1). An alternative arrangement could feature bound chains with additional alkanethiols interspersed but not chemically bonded to the V_2O_5 substrate, which could potentially provide a means of attaining the density of the bulk system, while adapting to the limitations of the surface, albeit with a significant loss in thiol-surface binding energy. Note finally that we arbitrarily use a single-layer model for the V_2O_5 (010) substrate. Irrespective of the number of layers, which is typically two in synthesized gels,²¹ the same two (010) faces will be exposed for the chain attachment.

Choice of Film Density in the Molecular Models. We use a doubled V_2O_5 unit cell³⁰ (Figure 1a(i)) as the substrate repeat unit in our models, with an area of $2 \times 1.148 \times 0.355 \text{ nm} = 0.82 \text{ nm}^2$. Onto this we graft 5 alkanethiols (Figure 1a(ii)), 2 on one face and 3 on the other (Configurations A and B) or 4 on one face and 1 on the other (Configuration C). For an interlamellar spacing of approximately 2.0 nm, giving extreme interdigitation, (Figure 1b), the densities sum to give 5 chains per 0.82 nm^2 or 6.1 chains/ nm^2 .

Table 1. Computed Film Stabilities (kcal/mol) in Dodecanethiol-V₂O₅ Nanostructures for Two Film Geometries and a Range of Interlayer Spacings and Chain Binding Arrangements^a

interlayer space (nm)	chain binding scheme	film energies per dodecanethiol chain			nonbonded components	
		bonded	nonbonded	sum	horizontal	vertical
Interdigitated Film Geometry						
2.0	A	+26.6	-13.4	+13.2	-4.4	-9.0
2.5		+25.2	-15.2	+10.0	-7.8	-7.4
3.0		+26.2	-10.2	+15.9	-9.2	-1.0
2.0	B	+26.0	-14.5	+11.5	-5.2	-9.3
2.5		+25.2	-15.2	+10.0	-7.3	-7.9
3.0		+26.2	-10.6	+15.6	-9.5	-1.1
2.5	C	+25.4	-15.4	+9.9	-10.9	-4.5
Control Simulations with Noninterdigitated Film Geometry						
2.5	A	+32.3	-16.9	+15.4	-14.0	-2.9
2.5	A*	+32.1	-17.0	+15.1	-14.4	-2.6
2.5	B	+32.4	-17.4	+15.0	-14.5	-2.9
2.5	C	+31.9	-17.9	+13.9	-15.8	-2.1

^a Total film energies obtained at 2.5 nm layer spacing are given in bold. Film energies are computed from the final 2 ns (1000 structures) of 5 ns room temperature molecular dynamics; full computational details are in the Supporting Information, section S1.5. A minus sign indicates film stabilisation. Time-averaged standard deviations are <0.2 kcal/mol. Chain attachment schemes are described in the text. Bonded and nonbonded energy terms quantify the conformational energy of the chains and the packing interactions between the chains. The large positive bonded terms reflect the inherent strain in alkanethiol assemblies, with similarly large bonded energy terms of 25.7 ± 0.1 kcal/mol computed for bulk dodecanethiol chains.³⁸ Non-bonded components are computed by averaging over the chains along each substrate face (horizontal) and between chains on opposing faces (vertical).

Figure 1c plots the maximum density available to the surfactant chains in both two- and three-dimensional space. The plot shows that, for interlamellar space >2.25 nm, each face has a grafting density lower than the 5.5 chains/nm² of a reference water-solvated dodecanethiol bilayer. Details of the water-solvated bilayer model will be presented elsewhere. In the dodecanethiol-V₂O₅ structures, only where the chains from the two layers overlap can one speak of an equivalent of 5 chains per layer (6.1 chains/nm²). In this overlap region, the dodecanethiol concentration is higher than elsewhere; this point on the film inhomogeneity is developed further in the Supporting Information, section S2. The decrease in density toward that of the water-solvated bilayer then directs widening of the interlamellar space; the 6.1 chain/nm² system at 2.0 nm (Figure 1b) corresponds to an overpacked system as reflected in the film energies in Table 1. As shown in Figure 1c, the reduced chain densities obtained in expanded interlamellar spaces directs the system toward a moderate spacing of 2.26 nm, which is in reasonable agreement with the microscopy image estimates of 2.40–2.55 nm from Figure 2. By switching to densities expressed in units of g/cm³ to compare with the known density of dodecanethiol bulk liquids, 0.85 g/cm³ at room temperature from^{31,32} Figure 1c shows that the three-dimensional chain density at a separation of 2.5 nm is 0.82 g/cm³, which is in very good agreement with the bulk liquid.

Layering stabilizes the system by increasing the density and maximizing packing. The narrow 2.0 nm interlamellar spacing gives a three-dimensional density that is approximately the sum of the individual densities of the three and two chains on alternating layers giving a total of five chains in the interlamellar space. This narrow 2 nm spacing results in overly cramped intercalated films. At 2.5 nm separation, the density at either face is lower than the bilayer system while at the interface or vertical center of the bilayer, the density is above the bilayer density. Together these horizontal and vertical packing effects combine to

provide an overall density that approximates the density of the bulk dodecanethiol liquid. The surfactant concentration used in the molecular dynamics models then corresponds, at the observed 2.5 nm interlamellar space, to a chain density similar to that of the reference systems. That is, it approximates the optimized two- and three-dimensional packing arrangements of the water-solvated bilayer and bulk liquid.

Molecular Dynamics Protocol. Each model was relaxed using 2000 steps of steepest descent minimization with respect to the CHARMM force field³³ and then brought to room temperature by gradually raising the temperature from 0 to 295 K over 2 ns of dynamics, while simultaneously loosening positional constraints on the alkanethiol chains. Substrate atoms were fixed to their crystallographic positions³⁰ throughout the simulations. The crystal structure of V₂O₅ in the V₂O₅·nH₂O xerogel is very similar³⁴ to the bulk V₂O₅ structure, and it is assumed that atomic positions are also similar. Vanadium and oxygen atoms were assigned van der Waals's radii from the V₂O₅ crystal contacts³⁰ with well depths corresponding to typical metal and oxygen parameters.³⁵ Each of the 11 models listed in Table 1 was then subjected to five nanosecond (5 ns) dynamics runs to allow for the formation of well-equilibrated film structures. This corresponds to 77 ns of dynamics, composed of 22 ns for equilibration plus 55 ns of equilibrated dynamics.

The NAMD program³⁶ was used to calculate Langevin dynamics with a constant volume–temperature ensemble. Periodic boundary conditions were applied with Ewald summation used to calculate the electrostatic interactions and a 2 fs time step used for dynamics by constraining covalent bonds to hydrogen via the ShakeH algorithm.³⁷ We recently used a similar simulation protocol^{35,38,39} to describe alkanethiol self-assembled monolayers on gold.⁴⁰ Image generation and Tcl script-based trajectory analysis was performed using the VMD program.⁴¹ The NAMD³⁶ scripts used for the simulations, together with the

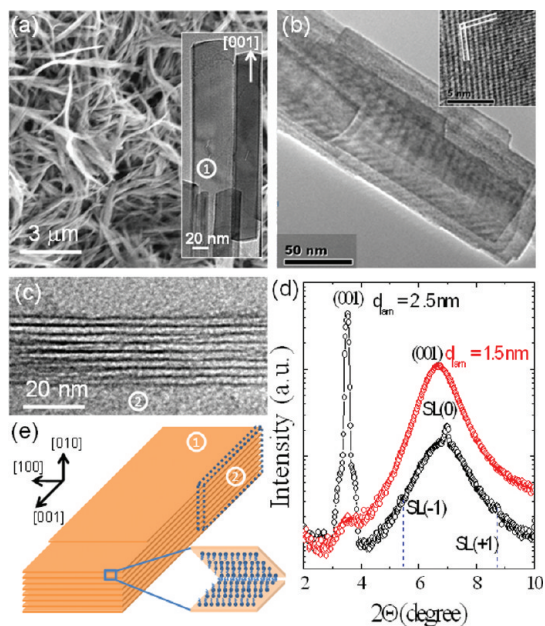


Figure 2. (a) SEM image of as-synthesized V₂O₅ nanofibers; (inset) plan view TEM image of several crystalline nanofibers. (b) Plan view TEM of several nanofibers overlapping; (inset) HRTEM image showing the single crystal nature of the nanofiber. (c) HRTEM image of the cross section of a single nanofiber showing the ordered, layered structure. The interlayer spacing is 2.40–2.55 nm. (d) Low angle X-ray diffraction (XRD) spectra of both the V₂O₅ xerogel and the V₂O₅-alkanethiol layered product acquired with grazing incidence geometry. (e) Schematic representation of the layered nanostructure. Regions 1 (plan view) and 2 (cross-section) correspond to the TEM images in panels a and c, respectively.

computed structures, are available on request from the corresponding author.

Next-generation models would benefit from (a) a combined quantum/classical approach that could simultaneously treat the substrate electronic structure and binding/unbinding of alkanethiols and solvent molecules, while (b) allowing for dynamic redistribution of alkanethiols between those that are chemically bound, those physisorbed to the substrate, and those in bulk-like states outside the fiber, within a constant pressure–temperature ensemble. Such complex, large, and long simulations are becoming more feasible with advances in high-performance computing.

RESULTS AND DISCUSSION

Alkanethiol-V₂O₅ Nanofiber Characterization. Figure 2a shows the as-synthesized V₂O₅ nanofibers. The dried layered fibers were synthesized as described above. After mild sonication to debundle the V₂O₅-thiol nanofibers, plan view transmission electron microscopy (TEM) images show the layered nature of these 2-dimensional crystals. Nanofibers are found to grow along the [100] direction (Figure 2a,b) and are single crystal in nature, as shown in the HRTEM image in Figure 2b, with lattice spacings corresponding to orthorhombic V₂O₅. Cross-sectional analysis of a single nanofiber by HRTEM (Figure 2c), summarized schematically in Figure 2e, clearly identifies the ordered layered structure, with well-defined interlayer spacings from this image in the range of 2.40–2.55 nm. Low angle XRD measurements in Figure 2d confirm this. The diffraction pattern is consistent with

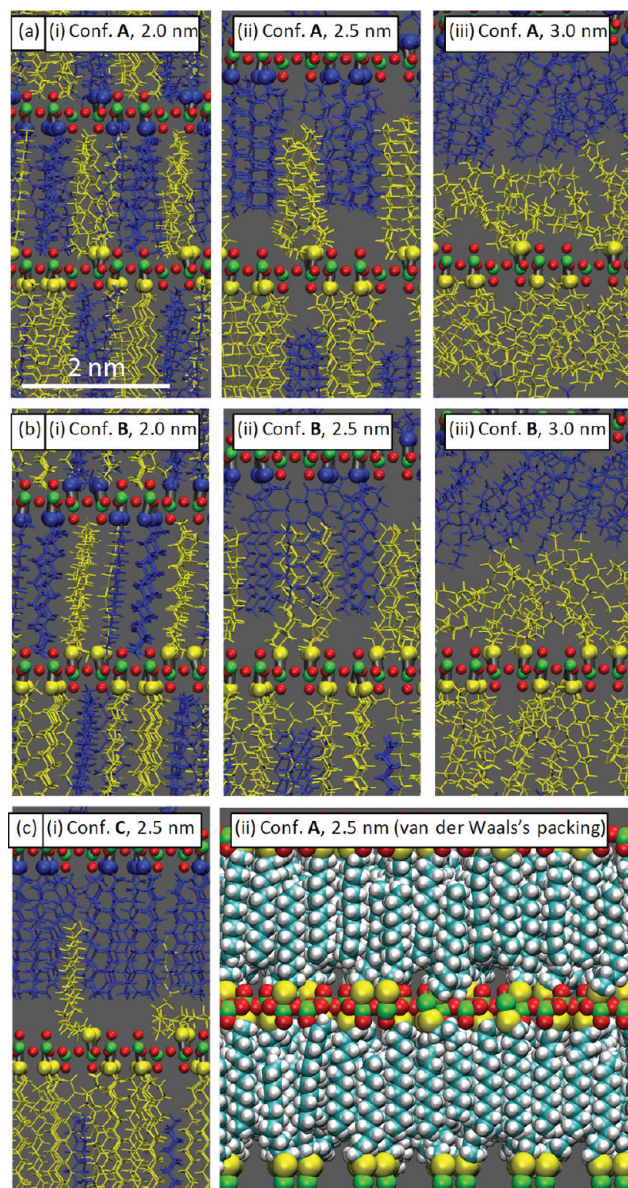


Figure 3. Panels a, b, and c (i) show representative molecular dynamics snapshots. Only chains within ± 3 nm of the center are shown, with chains on opposite substrate faces colored blue and yellow. Chains are shown as bonds with a terminal sulfur sphere, while V₂O₅ (010) is shown as green vanadium and red oxygen spheres. Panel c (ii) shows an alternative representation of one model with space-filling spheres.

the intercalation of the alkanethiol surfactant template into the layered matrix to form an effective double bilayer sandwich, and shows that the inorganic layered structure of the host xerogel is maintained consistent with a topotactic reaction. The (001) reflection for the V₂O₅-alkanethiol compound corresponds to a layer distance of ~ 2.5 nm, with the corresponding (001) reflection for the preliminary V₂O₅·nH₂O xerogel giving a much shorter interlayer spacing of ~ 1.5 nm (due to intercalated water). The highly layered nature of the hybrid V₂O₅-alkanethiol superlattice is observable from Figure 2d, where superlattice reflections SL(−1) and SL(+1) around a zeroth order SL(0) are found and are related to the intercalated bilayered alkanethiols sandwiched periodically between layers of V₂O₅ (010) faces.⁴²

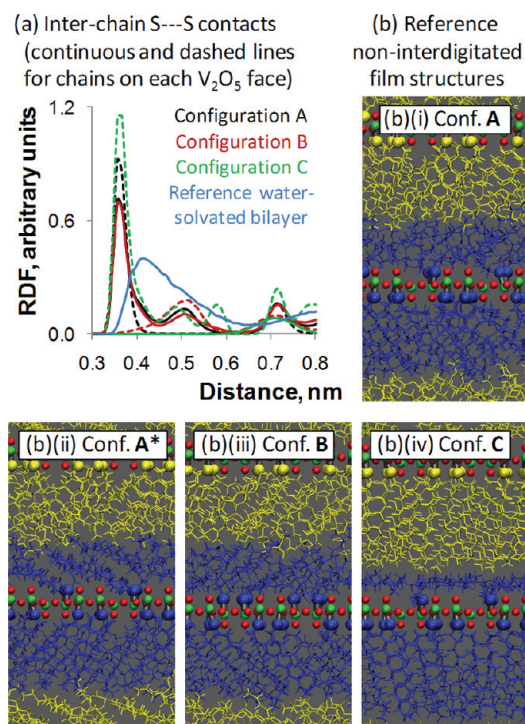


Figure 4. (a) Radial distribution functions (RDF) for thiol S–S separations on each substrate face compared with the perfect packing obtained in water. (b) Reference noninterdigitated structures in configurations (i) A, (ii) A*, (iii) B, and (iv) C.

X-ray photoelectron analysis of bulk nanofiber regions, where the majority of deposited fibers were found to be parallel to the substrate, indicate that they contain <10% V⁴⁺ (Supporting Information, Figure S3), and concentrations of V⁴⁺ up to 20% within the vanadium oxide layers will not alter the crystal structure of the material.¹⁹ This suggests effective functionalization of the opposing interlayer faces throughout the layer fibers. Finally, HRTEM analysis of fiber surfaces and cross-sections (Supporting Information, Figure S4) shows a thin 2–5 nm thiol layer at the edges of the nanofibers, consistent with non-V–S binding energies in the V 2p core level photoelectron spectra, indicating a small degree of physisorbed thiols on the outside of the fiber, which could stem from mild postsynthetic cleaning procedures.

Computed Structure, Dynamics, and Energetics of the Nanofiber. To quantify the effects of interlayer film spacing on the stability of the intercalated film using molecular dynamics simulations, 11 dodecanethiol-V₂O₅ models were used. The models were built with dodecanethiol chains grafted onto the (010) faces of the V₂O₅ crystal unit cell,³⁰ in three alternative binding configurations A (five models), B (four models), and C (two models), for a film density of 6.1 chains/nm² (Figure 1). Since the inorganic layers of the vanadium oxide are in fact molecular bilayers themselves,⁴² the organic docking surface remains identical with both faces juxtaposed in each interlayer gallery spacing. The 6.1 chains/nm² film density reflects the crystallography of V₂O₅ (010) as described previously in the Materials and Methods section. Note that similarly high densities in the range of 5.9–6.2 chains/nm² have been observed in alkanethiol assembly experiments on silver and gold/silver alloys.⁴³ For the monolayers described in ref 43, this excess

lateral density triggers defect formation in the substrate with the loss of long-range order. Our results below, however, show that vertically interdigitated bilayered films with this density on V₂O₅ favor the experimentally observed interlayer space. The computed molecular dynamics structures (Figure 3) then provide the atom-scale features of the layered structure revealed by electron microscopy (Figure 2).

In contrast to alkanethiol self-assembly on metals, the metal oxide V₂O₅ (010) substrate features oxygen-bridged vanadium binding sites.³⁰ This constraint gives the packing arrangements shown in Figure 3. The computed intersulfur distances given in Figure 4a show how, relative to a reference water-solvated dodecanethiol bilayer with S to S contacts of 0.41 nm,³³ the substrate imposes alternately cramped (0.37 nm) and sparse (0.51–0.72 nm) arrangements on the thiol headgroups.

We tested the plausibility of the interdigitated assembly by also considering an alternative model (Figure 4b) in which the chains tilt rather than interdigitate. These alternative models (listed in Table 1) use the chain attachment schemes A, B, and C (Figure 1a(ii)) with configuration A* also tested for the noninterdigitated model, an orientation whereby the monolayers are not aligned vertically but juxtaposed with opposing tilt angles. The computed preference for interdigitation is approximately -5 ± 1 kcal/mol per chain (Table 1, sum values). The tilted arrangement thus constitutes a very low probability state for the system. The preference arises largely from relief of molecular strain in the interdigitated film, by -7 kcal/mol per chain (Table 1, bonded terms), and is consistent with the upright chains observed in tunnelling microscopy images.²¹

Interdigitation then relieves conformational strain in the organic bilayer. Packing effects are less important, with the 6 ± 2 kcal/mol loss in horizontal ordering in the interdigitated geometry offset by the -4 ± 2 kcal/mol improvement in vertical contacts (Table 1, nonbonded components). Furthermore, the 2.5 nm structure promotes the moderate interdigitation that, relative to shorter 2.0 and longer 3.0 nm spacings, both minimizes strain and also improves interchain packing to within 2 kcal/mol of the noninterdigitated arrangement (Table 1, nonbonded terms). The 2.5 nm interdigitated film maximizes film contacts, both horizontally along each substrate face and vertically between opposing substrate faces; for long-range layered order in these directions, an alkanethiol density that equates to bulk, substrate-free two- and three-dimensional chain assemblies (Figure 1c) in addition to interdigitation is important. This three-dimensional packing under the constraint of the V₂O₅(010) crystallography underlies the formation of stable intercalated films with the observed ~ 2.5 nm interlayer distances (Figure 2c); the stability of the intercalated organic bilayer is primarily dictated by optimized packing densities. This value is in between once and twice the length of a free extended dodecanethiol molecule (1.5 nm), highlighting the reduction in the interlayer space due to interdigitation.

The film stabilization energies in Table 1 indicate a strong preference for the observed 2.5 nm interlayer spacing for both of the alternative chain attachment schemes A and B, in agreement with the available microscopy and diffraction data (Figure 2 and ref 21). The intermediate interlayer space of 2.5 nm gives a significantly more stable film, with chain energies improved by 2–6 kcal/mol, stemming from 1 to 2 kcal/mol benefits in chain conformations and also 1–5 kcal/mol from chain packing. The largest penalties are for widening rather than narrowing the interlayer space. Components show that the strongest driver

toward 2.5 nm is the \sim 7 kcal/mol improvement in vertical chain interdigitation compared to the wider 3.0 nm structure. Smaller benefits of 2–3 kcal/mol are obtained in horizontal chain packing along each substrate face for 2.5 nm rather than the narrower 2.0 nm spacing. Consideration then of the full three-dimensional packing explains the origin of the observed 2.5 nm spacing with the requirement of a minimal packing density of the thiols on V_2O_5 (010) and chain interdigititation to form the energetically preferable layered structure. The small empty pockets in the computed film structure (Figure 3c(ii)) are a consequence of the dry environment approximation used in the simulations with all alkanethiols bound to the substrate. These spaces may be occupied by solvent molecules in the experimental synthesized fibers; for further discussion of chain hydration and chain physisorption/diffusion in alkanethiol monolayers see refs 35,38, and 39, while vanadate surface hydration, including chemisorption, is addressed in electronic structure studies, see for example, refs 23 and 24.

Conformational and packing effects share the penalties for narrowing of the interlayer space to 2.0 nm, with chain conformation contributing 45% in A and 51% in B (Table 1). For widening the space to 3.0 nm, the packing penalty predominates, at 84% in A and 82% in B. The balance of film conformation and packing effects is thus almost independent of the chain attachment scheme. Arrangement C serves as the first approximation to a surface model with a mixture of reduced V^{4+} and stoichiometric V^{5+} sites,^{21,44} which may favor a situation whereby for example, 4 of the 5 chains per $[V_2O_5]_4$ unit point in the same direction to accommodate the large V^{4+} ion. The observed <10% V^{4+} , means such C arrangements will have a low population in the fiber. In terms of packing, C has both the lowest horizontal penalty and lowest vertical benefit (Table 1, nonbonded components) compared with those of A and B. This reflects the V^{4+} -directed alternately sparse/dense distribution of chains on opposing faces as shown in the thiol S–S separations in Figure 4a. The computed film energies reflect the delicate balance between horizontal and vertical packing.

Atom-Scale Origin of the 2.5 nm Interlayer Spacing. Overall, the data shows how the interlayer spacing of 2.5 nm arises from a combination of optimized (a) chain orientations and horizontal, substrate-constrained contacts along each substrate face and (b) vertical contacts between faces. The most important insight from the data is that surfactant packing is one of the primary directors and maintainer of interlayer spacing. For all binding schemes A, B, and C, the simultaneous optimization of packing in three dimensions stabilizes the interlayer film. The three alternative arrangements A, B, and C are essentially iso-energetic; all three may contribute to the layered structure. The optimal packing arrangement of the dodecanethiol chains is thus not a single periodic arrangement on V_2O_5 (010) but rather a mixture of states, lowering the sensitivity of the intercalated organic bilayer to the fine details of the substrate crystallography; the nature of the interlayer film directs the order in the layered structure. Organic layer defects³⁹ and the vanadate hydration state^{45,46} may also affect the ultimate arrangement. The findings will also motivate extensions to account for detailed thiol binding and unbinding and also dynamic redistribution of alkanethiols between those that are chemically bound, those physisorbed to substrate, and those in bulk-like states outside the fiber, toward a highly descriptive model for V_2O_5 -alkanethiol assembly and ultimately organic–inorganic hybrid layered materials in general.

The V_2O_5 directed surfactant assembly results in unusual three-dimensional packing arrangements that differ significantly from self-assembled monolayers formed on layered silicate and metal surfaces.^{27,40,47} In some features, the alkanethiols intercalated in V_2O_5 more resemble the molecular coats on low-diameter, curved nanoparticle surfaces.^{48–50} The molecular dynamics model thus confirms and extends the major features observed in the microscopy experiments; in vanadium oxide-alkanethiol structures synthesized from gels, the film assembly dictates a 2.5 nm interlayer spacing. The simulations confirm that the lowest energy film is neither a simple bilayer nor a juxtaposition of two monolayers. The film forms an interdigitated structure, in agreement with near-atom scale microscopy images²¹ that show the surfactant chains in upright orientations in the 2.5 nm space. This arrangement, when stacked as a superlattice, forms the layered structure, with the vertical interdigitation of alkanethiols offsetting the horizontal packing penalty induced by the oxygen-bridged vanadium binding sites.

CONCLUSIONS

The application of nanostructures in devices depends on the ability to organize them in complex architectures, so atomic-scale descriptions may speed up development.^{51,52} In the present work, we presented new information on film structure in layered vanadium oxide, specifically the interdigitation between monolayers on each substrate face to give the observed short interlayer spacing. One further experimental test of the proposed interdigitated model could involve STM characterization of exfoliated layers to show the organic monolayer on the vanadium oxide basal plane. Harnessing these subtle nanoscale effects may aid the production of nanostructured hybrid materials with physicochemical and mechanical properties tailored for specific device applications. For example, a layered oxide structure could be engineered to have, in an organic solvent, noninteracting layers that become tightly coupled upon drying, a possible new nanomaterial for adhesives. For energy conversion and storage materials, disentanglement of interdigitated films could be exploited to give a transducer that converts heat to mechanical energy. In the nearer term, hybrid materials that uptake nanoparticles or sieve/intercalate ions (e.g., lithium-ion battery materials and sensors) may benefit from controlled interlayer spacings for better filtration or incorporation of other inorganic materials. We hope that the results presented will motivate further studies of vanadate and other layered structures toward rational design that uses atom-scale properties to direct architecture and function.

ASSOCIATED CONTENT

S Supporting Information. HRTEM of dodecylamine-templated V_2O_5 nanotube layers, further discussion of film density, XPS of deposited nanofibers, and HRTEM of surface thiol layers around nanofibers. This material is available free of charge via the Internet at <http://pubs.acs.org>.

AUTHOR INFORMATION

Corresponding Author

*E-mail: damien.thompson@tyndall.ie (D.T.); colm.odwyer@ul.ie (C.O'D.).

Present Addresses

[§]Laboratory of Computational Chemistry and Biochemistry, Departement für Chemie and Biochemie, Universität Bern, Freiestrasse 3, CH-3012 Bern, Switzerland.

ACKNOWLEDGMENT

We acknowledge support from Science Foundation Ireland (SFI) under the Tyndall National Access Programme, the INSPIRE program funded by the Irish National Development Plan 2007–2013, and the European Community's Seventh Framework Programme (FP7/2007–2013) under grant agreement no 213382 (FUNMOL). We acknowledge SFI for computing resources at the Tyndall National Institute and SFI/Higher Education Authority for computing time at the Irish Centre for High-End Computing.

REFERENCES

- (1) Sanchez, C.; Julian, B.; Belleville, P.; Popall, M. *J. Mater. Chem.* **2005**, *15*, 3559–3592.
- (2) Pileni, M. P. *Nat. Mater.* **2003**, *2*, 145–150.
- (3) Shi, S. F.; Cao, M. H.; Fle, X. Y.; Xie, H. M. *Cryst. Growth Des.* **2007**, *7*, 1893–1897.
- (4) O'Hare, D.; Khan, A. I.; Ragavan, A.; Fong, B.; Markland, C.; O'Brien, M.; Dunbar, T. G.; Williams, G. R. *Ind. Eng. Chem. Res.* **2009**, *48*, 10196–10205.
- (5) Alivisatos, A. P. *Science* **1996**, *271*, 933–937.
- (6) Lieber, C. M.; Lu, W. *Nat. Mater.* **2007**, *6*, 841–850.
- (7) Decher, G. *Science* **1997**, *277*, 1232–1237.
- (8) Tenne, R.; Margulis, L.; Genut, M.; Hodes, G. *Nature* **1992**, *360*, 444–446.
- (9) Sanchez, C.; Gross, D.; Soler-Illia, G. J. D. A.; Crepaldi, E. L.; Cagnol, F.; Sinturel, C.; Bourgeois, A.; Brunet-Bruneau, A.; Amenitsch, H.; Albouy, P. A. *Chem. Mater.* **2003**, *15*, 4562–4570.
- (10) Vossmeyer, T.; Raible, I.; Burghard, M.; Schlecht, U.; Yasuda, A. *Sens. Actuators, B* **2005**, *106*, 730–735.
- (11) Li, G.; Chu, C. W.; Shrotriya, V.; Huang, J.; Yang, Y. *Appl. Phys. Lett.* **2006**, *88*, 253503.
- (12) O'Dwyer, C.; Diaz, C.; Lavayen, V. *J. Solid State Chem.* **2010**, *183*, 1595–1603.
- (13) O'Dwyer, C.; Lavayen, V.; Tanner, D. A.; Newcomb, S. B.; Benavente, E.; Gonzalez, G.; Torres, C. M. S. *Adv. Funct. Mater.* **2009**, *19*, 1736–1745.
- (14) Coleman, J. N.; Lotya, M.; O'Neill, A.; Bergin, S. D.; King, P. J.; Khan, U.; Young, K.; Gaucher, A.; De, S.; Smith, R. J.; Shvets, I. V.; Arora, S. K.; Stanton, G.; Kim, H. Y.; Lee, K.; Kim, G. T.; Duesberg, G. S.; Hallam, T.; Boland, J. J.; Wang, J. J.; Donegan, J. F.; Grunlan, J. C.; Moriarty, G.; Shmeliov, A.; Nicholls, R. J.; Perkins, J. M.; Grieveson, E. M.; Theuwissen, K.; McComb, D. W.; Nellist, P. D.; Nicolosi, V. *Science* **2011**, *331*, 568–571.
- (15) Xia, Y. N.; Yang, P. D.; Sun, Y. G.; Wu, Y. Y.; Mayers, B.; Gates, B.; Yin, Y. D.; Kim, F.; Yan, Y. Q. *Adv. Mater.* **2003**, *15*, 353–389.
- (16) Park, J.; Lee, E.; Lee, K. W.; Lee, C. E. *Appl. Phys. Lett.* **2006**, *89*, X.
- (17) Baik, J. M.; Kim, M. H.; Larson, C.; Yavuz, C. T.; Stucky, G. D.; Wodtke, A. M.; Moskovits, M. *Nano Lett.* **2009**, *9*, 3980–3984.
- (18) Wu, C. Z.; Xie, Y. *Energy Environ. Sci.* **2010**, *3*, 1191–1206.
- (19) Livage, J. *Chem. Mater.* **1991**, *3*, 578–593.
- (20) Selloni, A.; Sun, C. H.; Liu, L. M.; Lu, G. Q.; Smith, S. C. *J. Mater. Chem.* **2010**, *20*, 10319–10334.
- (21) O'Dwyer, C.; Lavayen, V.; Fuenzalida, D.; Lozano, H.; Santa Ana, M. A.; Benavente, E.; Gonzalez, G.; Torres, C. M. S. *Small* **2008**, *4*, 990–1000.
- (22) Chirayil, T.; Zavalij, P. Y.; Whittingham, M. S. *Chem. Mater.* **1998**, *10*, 2629–2640.
- (23) Yin, X. L.; Han, H. M.; Gunji, I.; Endou, A.; Ammal, S. S. C.; Kubo, M.; Miyamoto, A. *J. Phys. Chem. B* **1999**, *103*, 4701–4706.
- (24) Thompson, D.; Hodnett, B. K. *Top. Catal.* **2008**, *50*, 116–123.
- (25) Casal, B.; Ruizhitzky, E.; Crespin, M.; Tiné, D.; Galvan, J. C. *J. Chem. Soc. Faraday Trans. 1* **1989**, *85*, 4167–4177.
- (26) Lavayen, V.; O'Dwyer, C.; Santa Ana, M. A.; Newcomb, S. B.; Benavente, E.; Gonzalez, G.; TorreS, C. M. S. *Phys. Status Solidi B* **2006**, *243*, 3285–3289.
- (27) Heinz, H.; Castelijns, H. J.; Suter, U. W. *J. Am. Chem. Soc.* **2003**, *125*, 9500–9510.
- (28) Parr, R. G.; Yang, W. T. *J. Am. Chem. Soc.* **1984**, *106*, 4049–4050.
- (29) Gronbeck, H.; Curioni, A.; Andreoni, W. *J. Am. Chem. Soc.* **2000**, *122*, 3839–3842.
- (30) Wyckoff, R. W. G. *Crystal Structures*; R.E. Krieger Publishing Co.: Malabar, FL, 1982.
- (31) *CRC Handbook of Chemistry and Physics*, 77th ed.; CRC Press: New York, 1996–1997.
- (32) Sigma-Aldrich 1-Dodecanethiol. http://www.sigmapelrich.com/catalog/ProductDetail.do?D7=0&NS=SEARCH_CONCAT_PNO|BRAND_KEY&N4=471364|ALDRICH&N25=0&QS=ON&F=SPEC (accessed July 26 2011).
- (33) MacKerell, A. D.; Bashford, D.; Bellott, M.; Dunbrack, R. L.; Evanescz, J. D.; Field, M. J.; Fischer, S.; Gao, J.; Guo, H.; Ha, S.; Joseph-McCarthy, D.; Kuchnir, L.; Kuczera, K.; Lau, F. T. K.; Mattos, C.; Michnick, S.; Ngo, T.; Nguyen, D. T.; Prodhom, B.; Reiher, W. E.; Roux, B.; Schlenkrich, M.; Smith, J. C.; Stote, R.; Straub, J.; Watanabe, M.; Wiorkiewicz-Kuczera, J.; Yin, D.; Karplus, M. *J. Phys. Chem. B* **1998**, *102*, 3586–3616.
- (34) Petkov, V.; Trikalitis, P. N.; Bozin, E. S.; Billinge, S. J. L.; Vogt, T.; Kanatzidis, M. G. *J. Am. Chem. Soc.* **2002**, *124*, 10157–10162.
- (35) Gannon, G.; Larsson, J. A.; Thompson, D. *J. Phys. Chem. C* **2009**, *113*, 7298–7304.
- (36) Phillips, J. C.; Braun, R.; Wang, W.; Gumbart, J.; Tajkhorshid, E.; Villa, E.; Chipot, C.; Skeel, R. D.; Kale, L.; Schulten, K. *J. Comput. Chem.* **2005**, *26*, 1781–1802.
- (37) Ryckaert, J. P.; Ciccotti, G.; Berendsen, H. J. C. *J. Comput. Phys.* **1977**, *23*, 327–341.
- (38) Gannon, G.; Larsson, J. A.; Greer, J. C.; Thompson, D. *Langmuir* **2009**, *25*, 242–247.
- (39) Gannon, G.; Greer, J. C.; Larsson, J. A.; Thompson, D. *ACS Nano* **2010**, *4*, 921–932.
- (40) Love, J. C.; Estroff, L. A.; Kriebel, J. K.; Nuzzo, R. G.; Whitesides, G. M. *Chem. Rev.* **2005**, *105*, 1103–1169.
- (41) Humphrey, W.; Dalke, A.; Schulter, K. *J. Mol. Graphics* **1996**, *14*, 33–&.
- (42) Giorgetti, M.; Passerini, S.; Smyrl, W. H.; Berrettoni, M. *Inorg. Chem.* **2000**, *39*, 1514–1517.
- (43) Kawasaki, M.; Iino, M. *J. Phys. Chem. B* **2006**, *110*, 21124–21130.
- (44) Avansi, W.; Ribeiro, C.; Leite, E. R.; Mastelaro, V. R. *Cryst. Growth Des.* **2009**, *9*, 3626–3631.
- (45) O'Dwyer, C.; Lavayen, V.; Newcomb, S. B.; Ana, M. A. S.; Benavente, E.; Gonzalez, G.; Torres, C. M. S. *J. Electrochem. Soc.* **2007**, *154*, K29–K35.
- (46) Livage, J. *Nat. Mater.* **2003**, *2*, 297–299.
- (47) Heinz, H.; Vaia, R. A.; Farmer, B. L. *Langmuir* **2008**, *24*, 3727–3733.
- (48) Badia, A.; Cuccia, L.; Demers, L.; Morin, F.; Lennox, R. B. *J. Am. Chem. Soc.* **1997**, *119*, 2682–2692.
- (49) Wang, L. Y.; Shi, X. J.; Kariuki, N. N.; Schadt, M.; Wang, G. R.; Rendeng, Q.; Choi, J.; Luo, J.; Lu, S.; Zhong, C. J. *J. Am. Chem. Soc.* **2007**, *129*, 2161–2170.

- (50) Wang, J. C.; Neogi, P.; Forciniti, D. *J. Chem. Phys.* **2006**, *125*, 194717.
- (51) Perl, A.; Gomez-Casado, A.; Thompson, D.; Dam, H. H.; Jonkheijm, P.; Reinoudt, D. N.; Huskens, J. *Nat. Chem.* **2011**, *3*, 317–322.
- (52) Noy, A. *Adv. Mater.* **2011**, *23*, 807–820.